Supplement of Atmos. Chem. Phys., 25, 16747–16774, 2025 https://doi.org/10.5194/acp-25-16747-2025-supplement © Author(s) 2025. CC BY 4.0 License.





Supplement of

Brown carbon emissions from laboratory combustion of Eurasian arcticboreal and South African savanna biomass

Arya Mukherjee et al.

Correspondence to: Arya Mukherjee (arya.mukherjee@uef.fi) and Olli Sippula (olli.sippula@uef.fi)

The copyright of individual parts of the supplement might differ from the article licence.

S1: Description of Fuels and combustion set up:

Samples of Finnish boreal forest surface (BFS), South African savanna grass and wood (SG and SW), and four different types of peat, including commercially available peat fuel (CP), natural peatlands from Finland (FIA and FIB), subarctic permafrost area of Russia (RUS) and arctic Svalbard peat from Norway (NOR) were used in the experiments (Table S1). Details of the savanna biomasses used in this study can be found in Vakkari et al. (2025), while details regarding the NOR, RUS, FIA and FIB biomasses have been described by Schneider et al., 2024.

Finnish boreal forest biomass and Arctic-boreal peats were selected for this study, specifically due to the lack of knowledge regarding aerosol emission from these biomasses. Furthermore, with ongoing climate warming, unprecedented wildfires have been recorded both in the boreal forest and Arctic and are projected to increase in the future (Jain et al., 2024; Descals et al., 2022). Boreal and particularly Arctic wildfires largely consume soil organic matter, in many cases consisting of peat (Huang and Rein, 2017; Walker et al., 2020). South African savanna biomasses, on the other hand, constitutes a major fraction of wildfire emissions from continental Africa and contributes significantly to global carbon emissions (Vakkari et al., 2018,2025; van Wees et al., 2022). Even though savanna wildfires are open surface fires, yet the emissions contain much more EC (or BC) compared to Eurasian biomasses, therefore allowing us a wider range to study the effects of BB emitted EC/OC on the optical properties of the emission. We also included a few data points in this study from modern European chimney stove emissions, which are classified as residential wood combustion (RWC) emissions. We have previously shown that modern RWC emissions are EC-rich (Mukherjee et al., 2024) due to their high combustion temperatures. Therefore, including these data points in the current study helped us explore the temperature and EC/OC continuum of biomass burning in three regimes such as:

1) the low temperature combustion of Arctic-boreal surface and corresponding OC-rich emissions, 2) the high temperature wood combustion and resulting EC-rich emissions and 3) the woody and grassy savanna fire emissions, which fall in between 1) and 2).

With that background, we then explored how these temperature continuum influence the BC-BrC continuum in the BB emissions along with their corresponding light absorption properties.

Savanna biomass was cultivated in the North-West University's garden in South Africa and delivered to Finland. The savanna biomass used in the study consisted of ten different species representing indigenous savanna biomass from South Africa, including: *Celtis africana*, *Searsia pyroides*, *Vachellia karroo*, *Ziziphus mucronata*, *Asparagus laricinus*, *Gymnosporia buxifolia*, *Euclea undulata*, *Senegalia caffra*, *Pavetta zeyheri*, *Vangueria infausta*, and *Zanthoxylum capense*. The savanna biomass was divided into grass and woody samples. The savanna grasses were burned in an upright position in 50 g batches without shortening or other modification of the samples. The burning samples of savanna trees were prepared as composite batches, including material from all savanna tree species for a total of 60 g. The savanna tree batches included thorns, leaves, and branches from the species. The savanna tree material was cut into smaller pieces to fit into the B and C sample holders marked in Figure S2(i).

Different sample holders were used for different biomasses in our experiments which are illustrated in Supplementary Fig. S2. Boreal forest surface (BFS) samples needed large piece of wire mesh below it on the open biomass burning setup to keep the sample intact so that it doesn't fall between the spaces on grate during long smoldering phase. BFS samples were burnt from top to bottom by placing a heating rod horizontally on top of the sample surface in order to mimick more natural progression of forest floor fires. Extra litters were present in each sample as found in a naural Finnish BFS.

Savanna and peat samples had the heating rod in the middle of the burned sample to provide more surface-area for the sample to heat up for the combustion experiment. Keeping the mass of combusted biomass same between different sample types of peat needed two different sample holder setups. CP, RUS and NOR samples were more dense and solid compared to FIA and FIB, which were more porous and fluffy in texture (Figure S2). Clam shaped (CP, Svalbard, savanna material) sample holder was used to keep the burning material close to the electrical resistor (heating rod), because during the combustion there was a possibility that burned material lost its shape and wasn't close enough to resistor to continue burning. This wasn't necessary for FIA, FIB and Russian sample types because they settled better on the heating rod. Minimal modifications were made to the samples before combustion to keep them as they were provided to us.

S2: Description of OC-EC analyses:

Thermal—optical carbon analysis with the IMPROVE-A protocol was carried out by placing a filter punch in the sample oven of a carbon analyzer. The filter punches were first heated in completely inert (100 % He) condition where various OC subfractions gradually volatilized at temperature ramps of 140 °C (OC1), 280 °C (OC2), 480 °C (OC3), and 580 °C (OC4). The system then switched to an oxidizing atmosphere (He with a fixed amount of O2) where EC subfractions combusted at 580 °C (EC1), 740 °C (EC2), and 840 °C (EC3). The released carbon compounds were converted to either carbon dioxide (CO2) or methane (CH4), followed by infrared absorption (CO2) or flame ionization (CH4) detection. During the thermal analysis, a fraction of OC pyrolyzed or charred (Pyrolyzed Carbon, PC) under the inert He atmosphere into EC-like substances and were accounted for using optical correction by reflectance. Specifically, the instrument monitored the sample filter reflectance throughout the analysis using a laser source. The filter reflectance decreased in response to the formation of PC and then increased as the PC was combusted off the filter. The split between OC and EC is defined as the point at which reflectance returns to its initial reading before the heating started. OC and EC data discussed in this work refer to those after the correction as per the following equations:

Corrected OC = OC1 + OC2 + OC3 + OC4 + PC

Corrected EC = EC1+EC2+EC3-PC

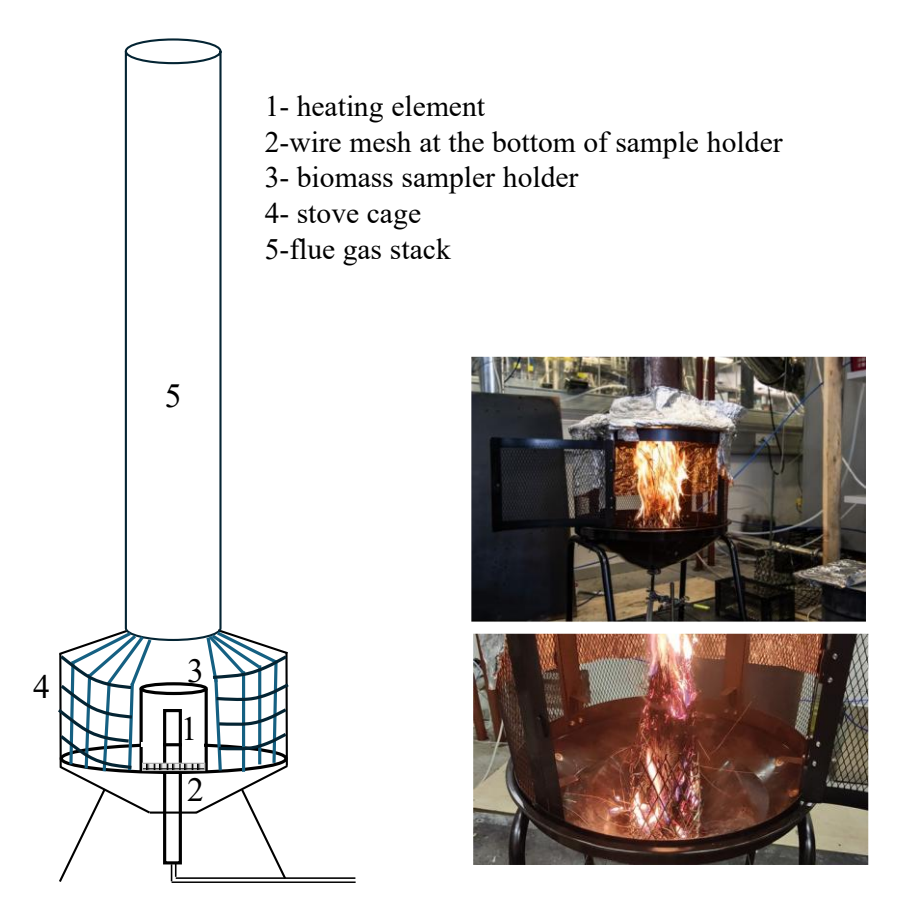


Figure S1: Graphical representation of the combustion set up with its 5 different components along with some pictures taken during the combustion experiments

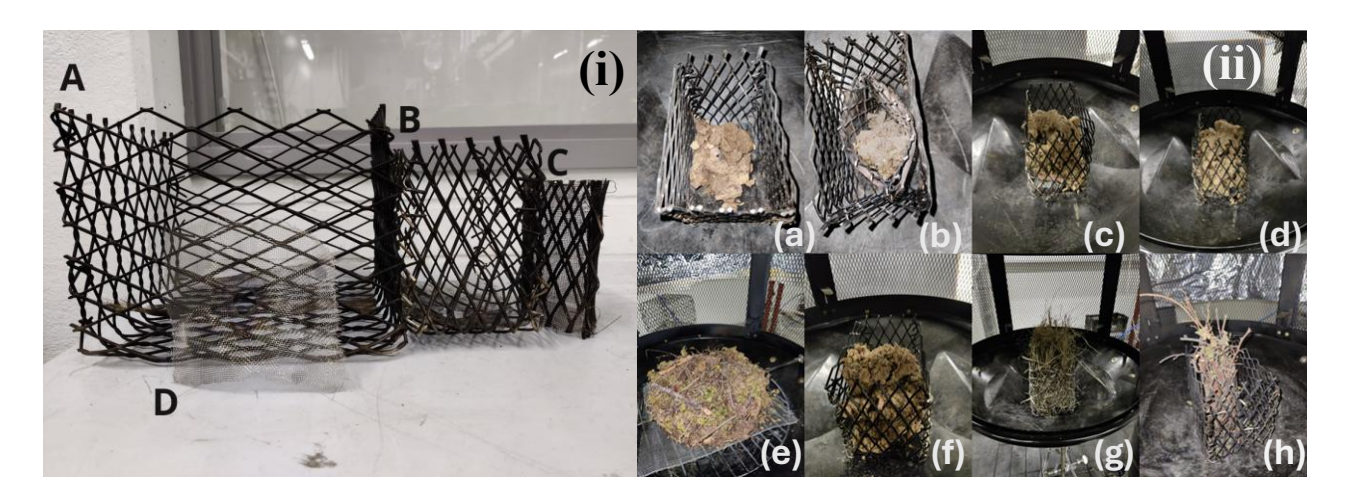


Figure S2: Pictures of different biomass holders used for the experiments. (i) *Left:* biomass holder for BFS samples (A), biomass holders (B and C) for savanna (SG) and peat samples (CP, FIA, FIB, RUS and NOR), and wired mesh used at the bottom of the holders (D); (ii) *Right:* Exemplary images of different biomasses in their respective holders before combustion; (a) Russian Peat, (b) Svalbard Peat (NOR), (c-d) Finnish peatlaland from Lakkasuo (FIA) (e) Boreal forest surface (BFS), (f) Finnish peatland from Siikaneva (FIB), (g) savanna grass (SG) and (h) savanna wood (SW)

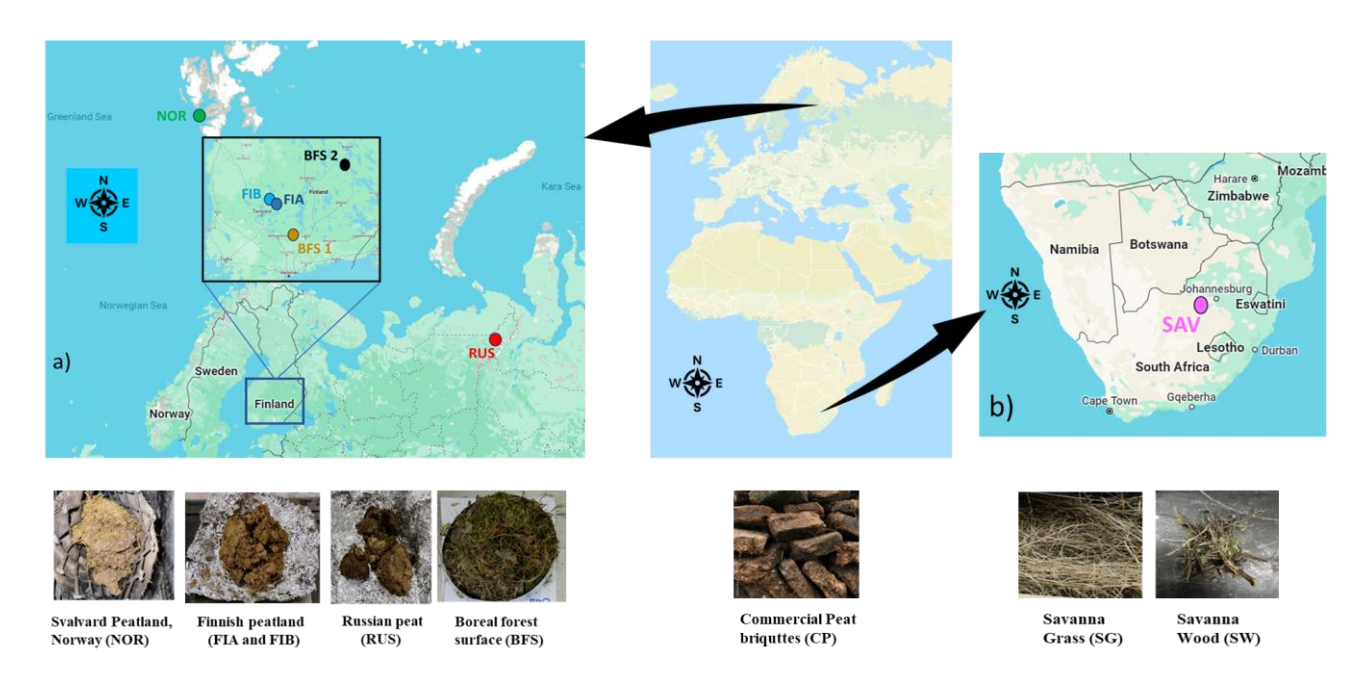


Figure S3: Geographic locations of the (a) Northern European Biomass and (b) South African savanna biomass used for this study (© Google maps 2025)

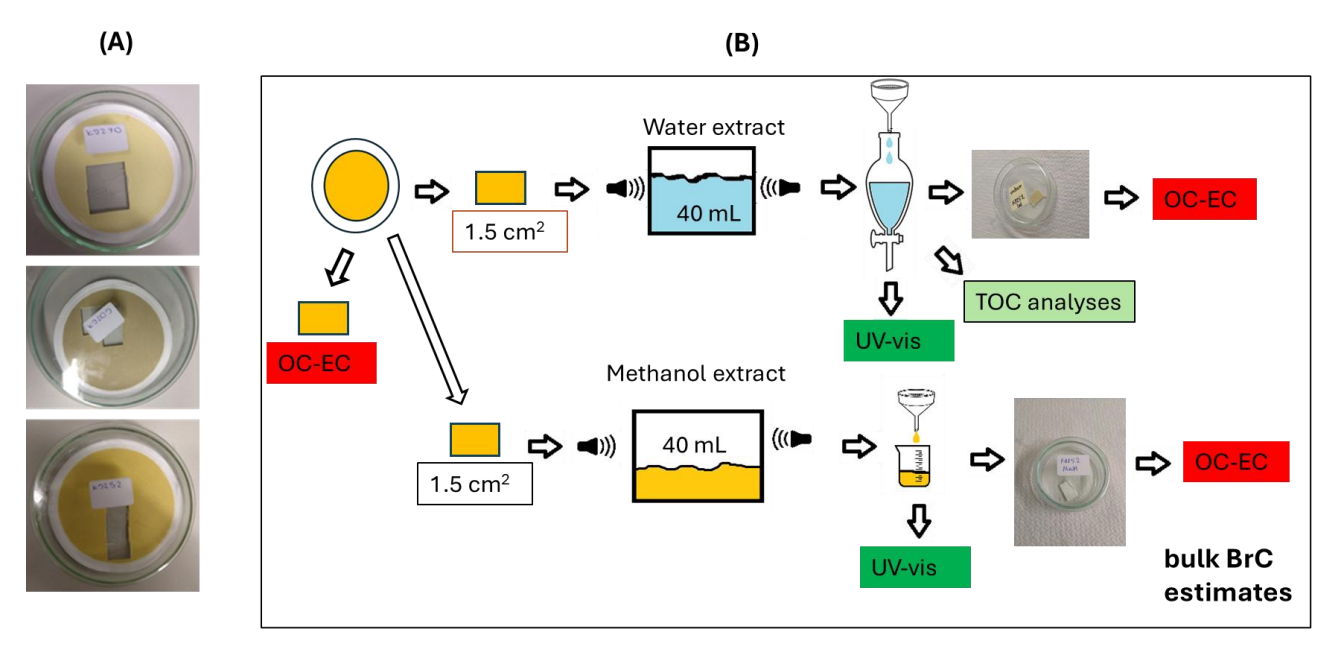


Figure S4: (A) representative images of 90 mm Quartz fiber filters collected for different fresh BB emissions and (B) graphical schematic of the extraction process for filters collecting fresh BB emissions

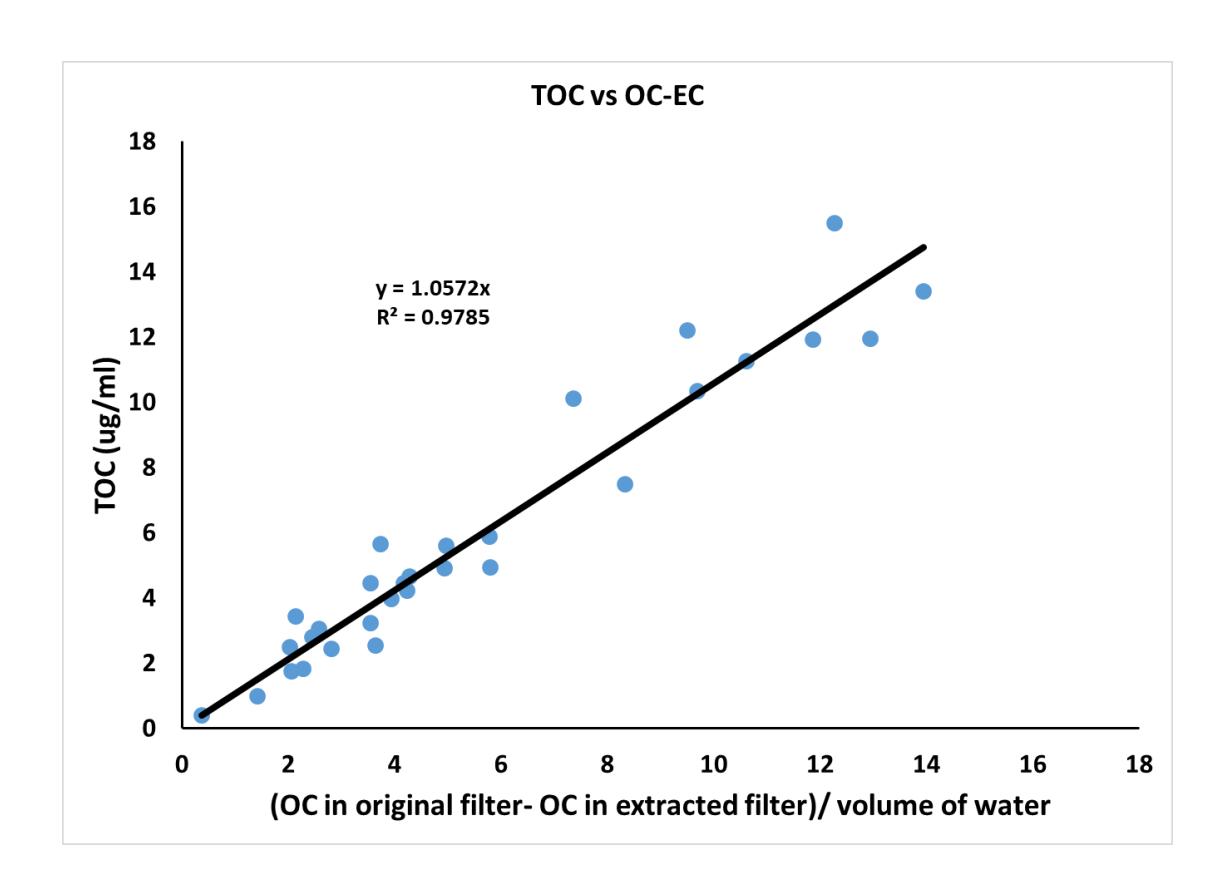


Fig. S5: Comparison between TOC and OC-EC analyzer based estimations of WSOC concentrations for fresh BB emissions

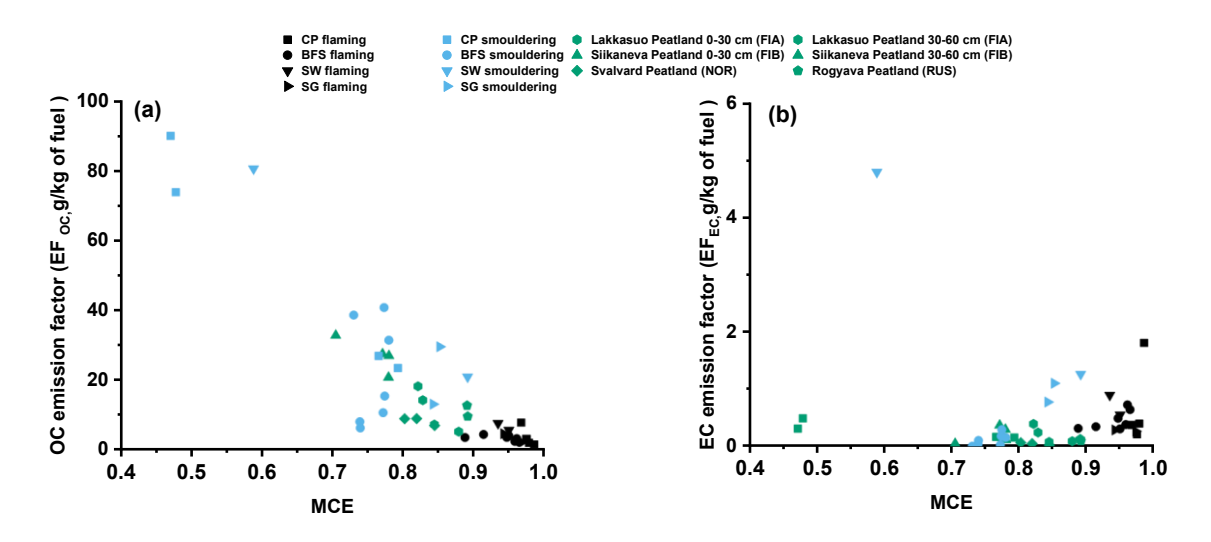


Figure S6: Dependence of EF_{EC} and EF_{OC} on MCE of the combustion

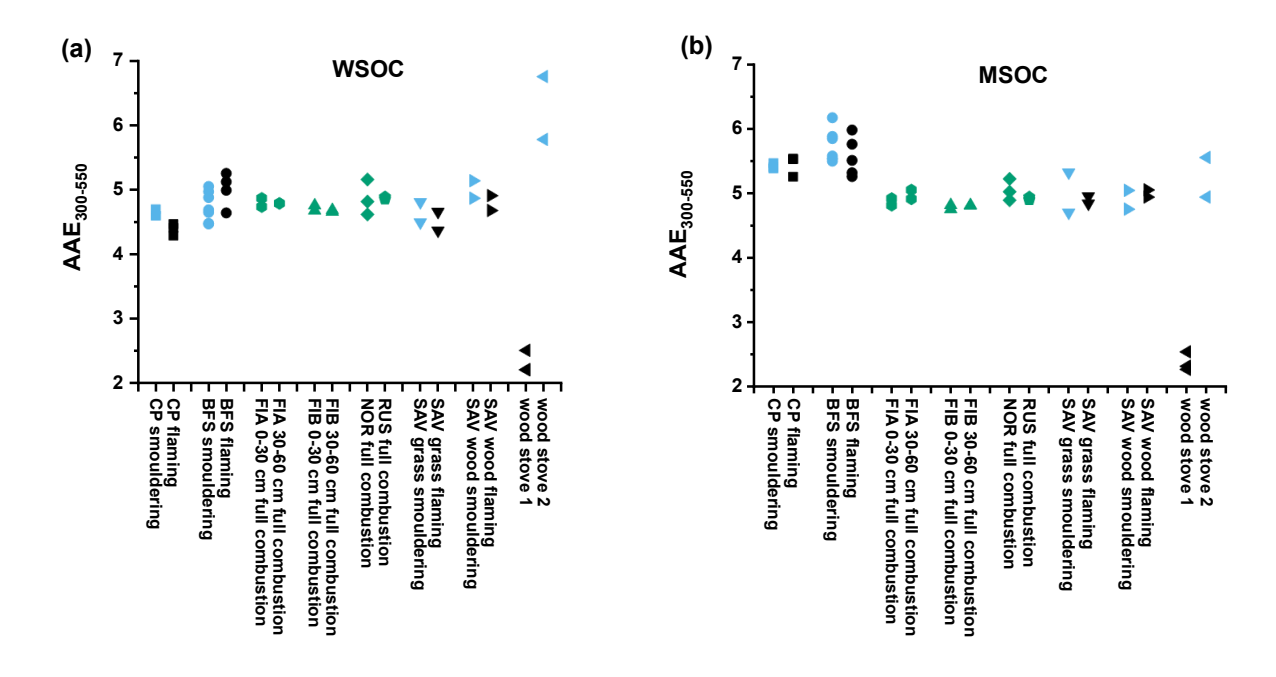


Fig. S7: AAE₃₀₀₋₅₅₀ for WSOC (a) and MSOC (b) of fresh BB emissions in this study

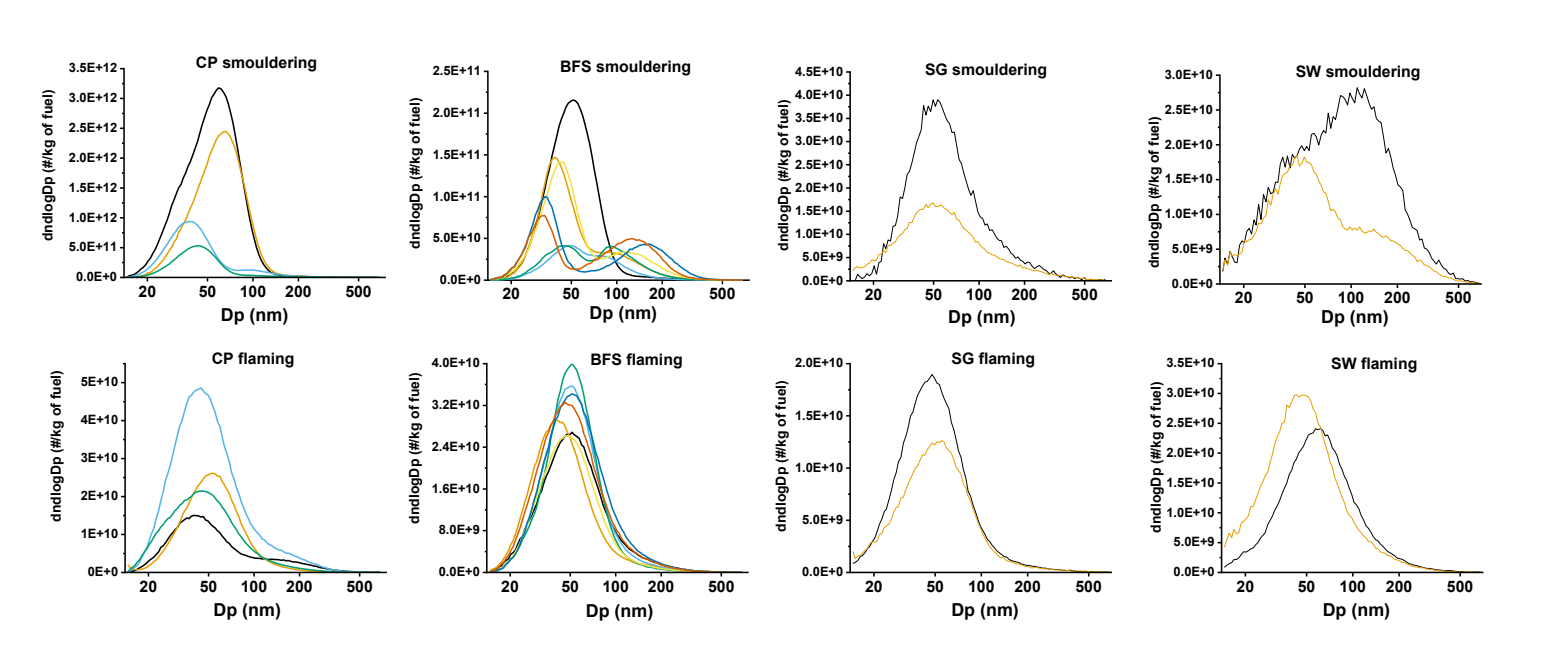


Fig. S8: particle number size distribution of different replicates of the environmental chamber experiments conducted in this study for smouldering and flaming burns of commercial peat (CP), Boreal Forest Surface (BFS), Savanna grass (SG) and savanna wood (SW)

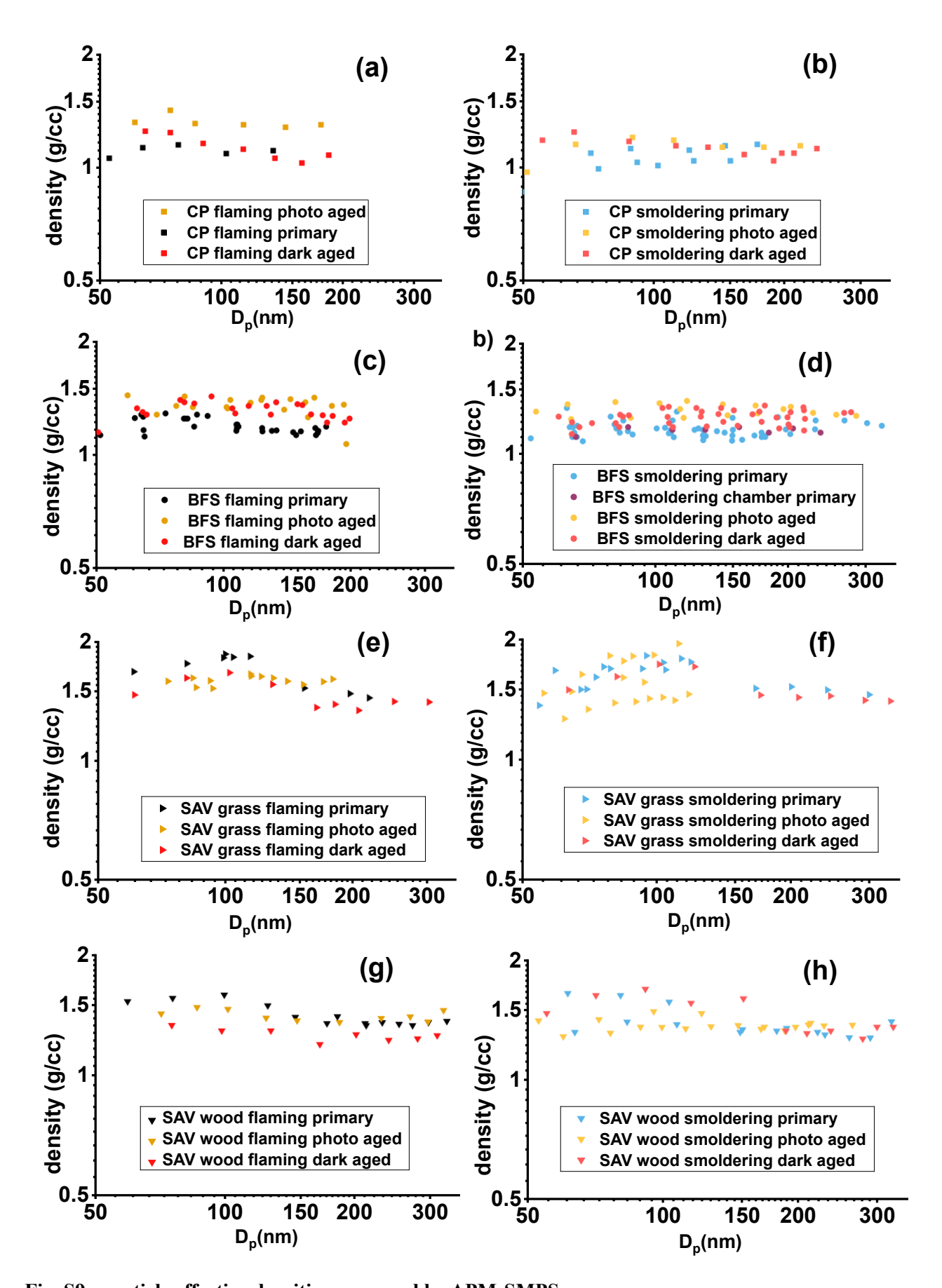


Fig. S9: particle effective densities measured by APM-SMPS

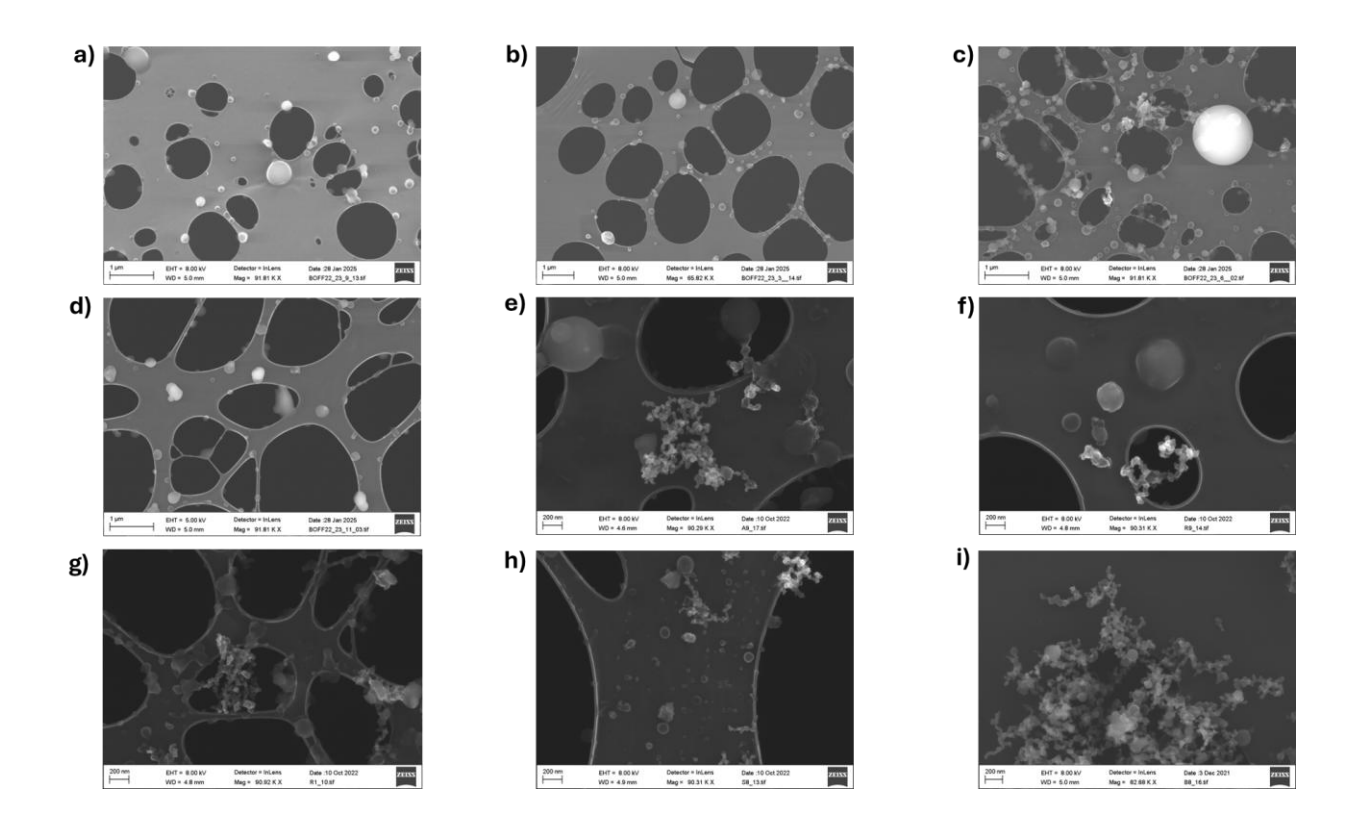


Fig. S10: Electron microscope images of primary particles from a) CP flaming, b) CP smouldering, c) BFS flaming, d) BFS smouldering, e) SG flaming, f) SG smouldering, g) SW flaming, h) SW smouldering and i) wood stove emissions

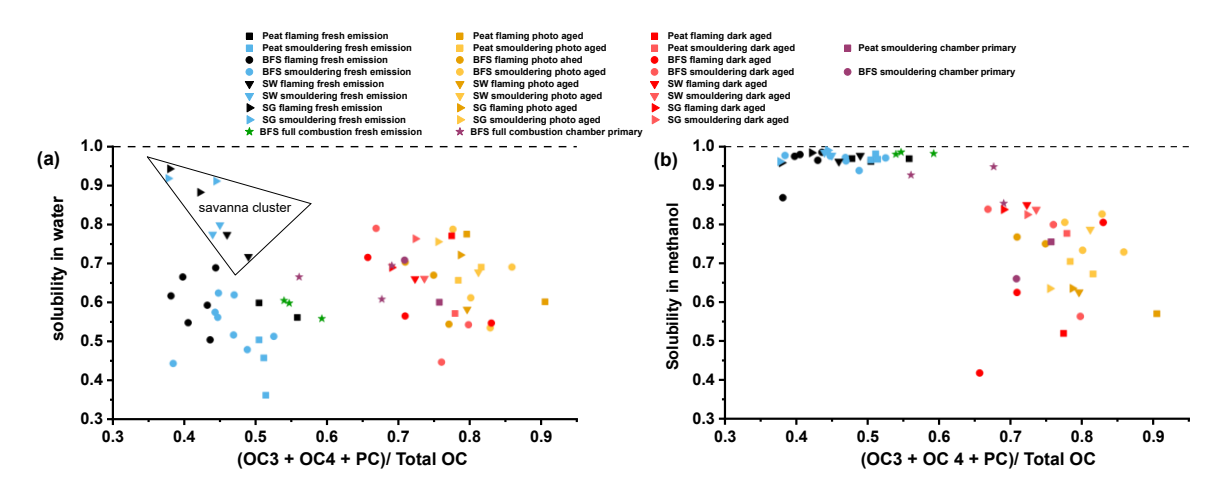


Fig. S11: Solubility of low volatile organics (OC3, OC4 and PC) in water (a) and MeOH (b) for fresh emission, chamber diluted primary emissions and photochemically and dark aged emissions in chamber for smouldering and flaming burns of CP (square) and BFS (circle) biomasses.

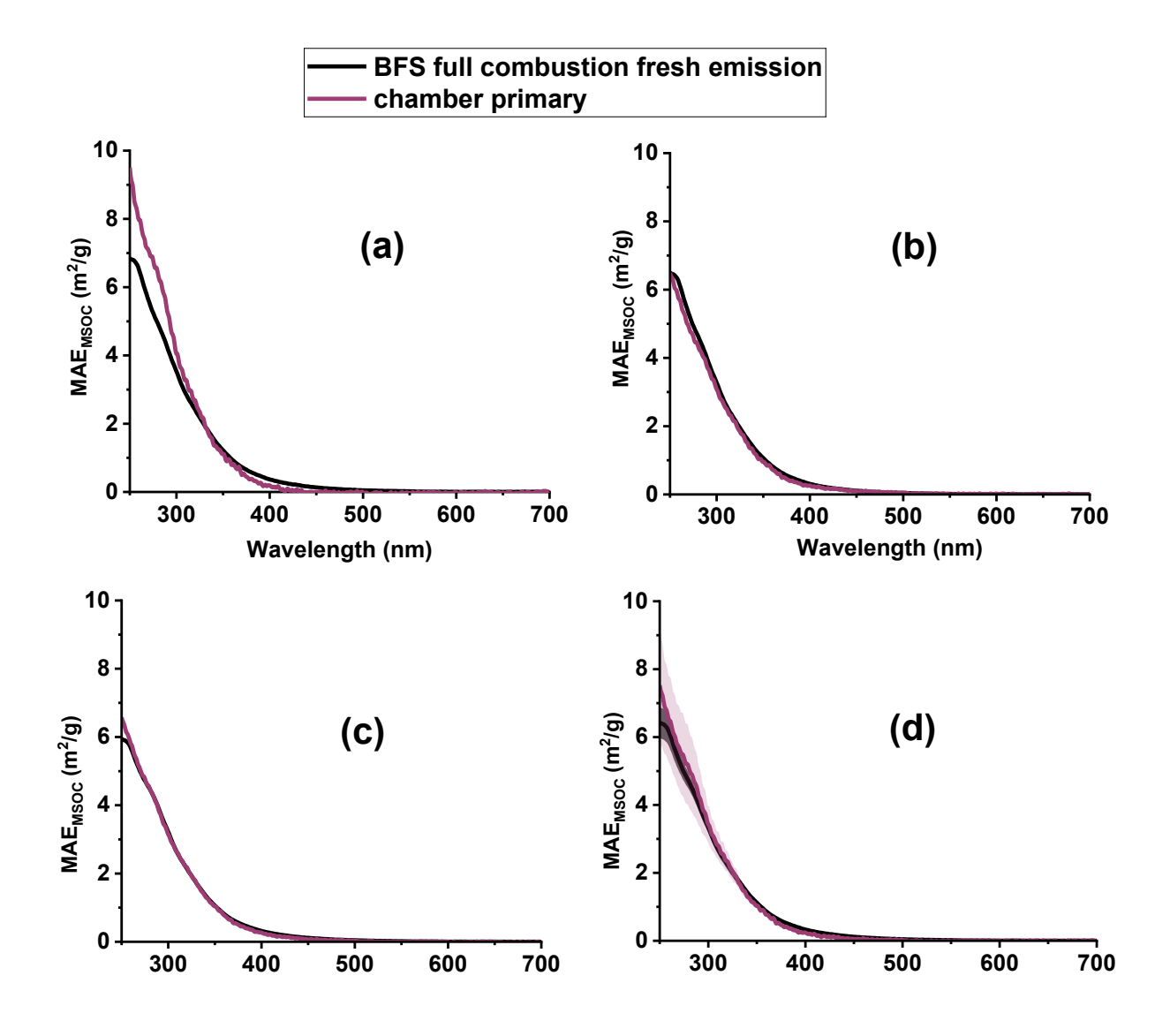


Fig. S12: Wavelength dependence of MAE_{MSOC} for fresh emission and chamber diluted primary samples from full combustion of BFS samples. (a-c) denote three separate replicates ,while (d) is the mean values (solid lines) of the three replicates and the standard deviation from mean (shaded area)

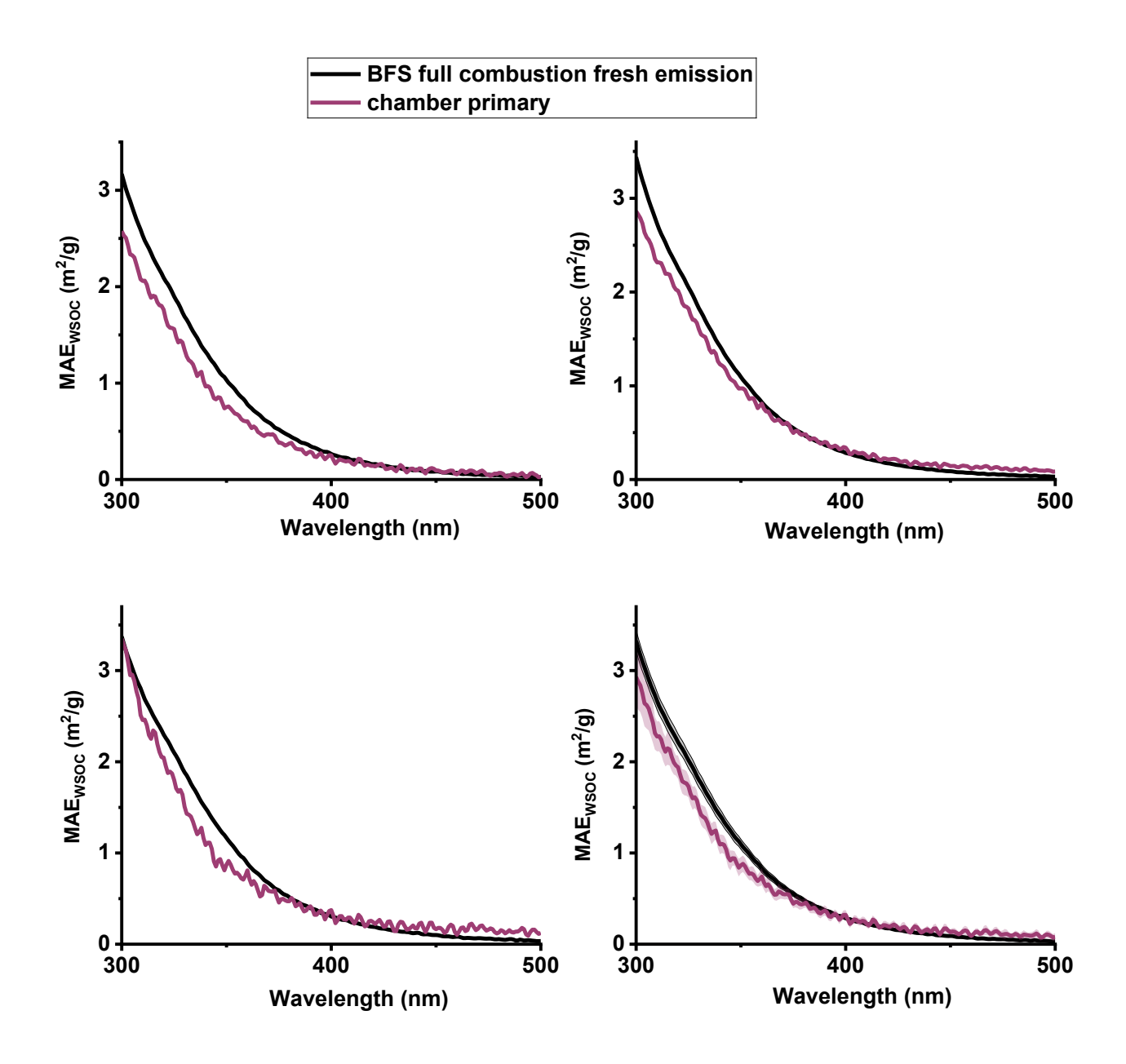


Fig. S13: Wavelength dependence of MAE $_{WSOC}$ for fresh emission and chamber diluted primary samples from full combustion of BFS samples. (a-c) denote three separate replicates, while (d) is the mean values (solid lines) of the three replicates and the standard deviation from mean (shaded area)

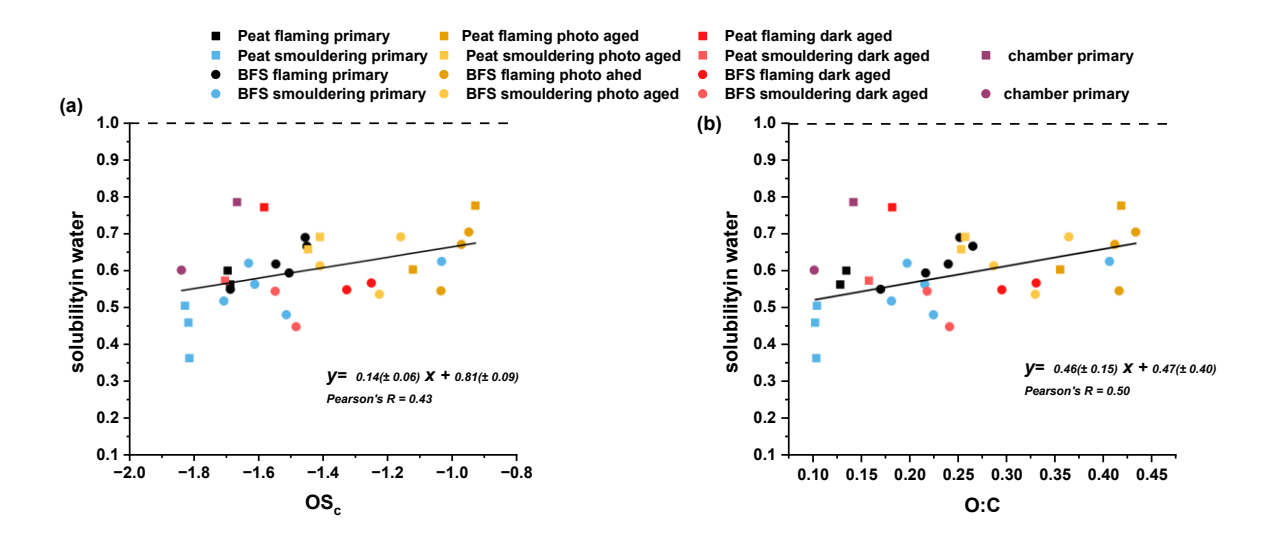


Fig. S14: solubility of OC in water (alternatively WSOC fraction of total OC) vs oxidation state of chamber diluted primary and aged particles (a) and O:C ratio of chamber diluted primary and aged particles (b)

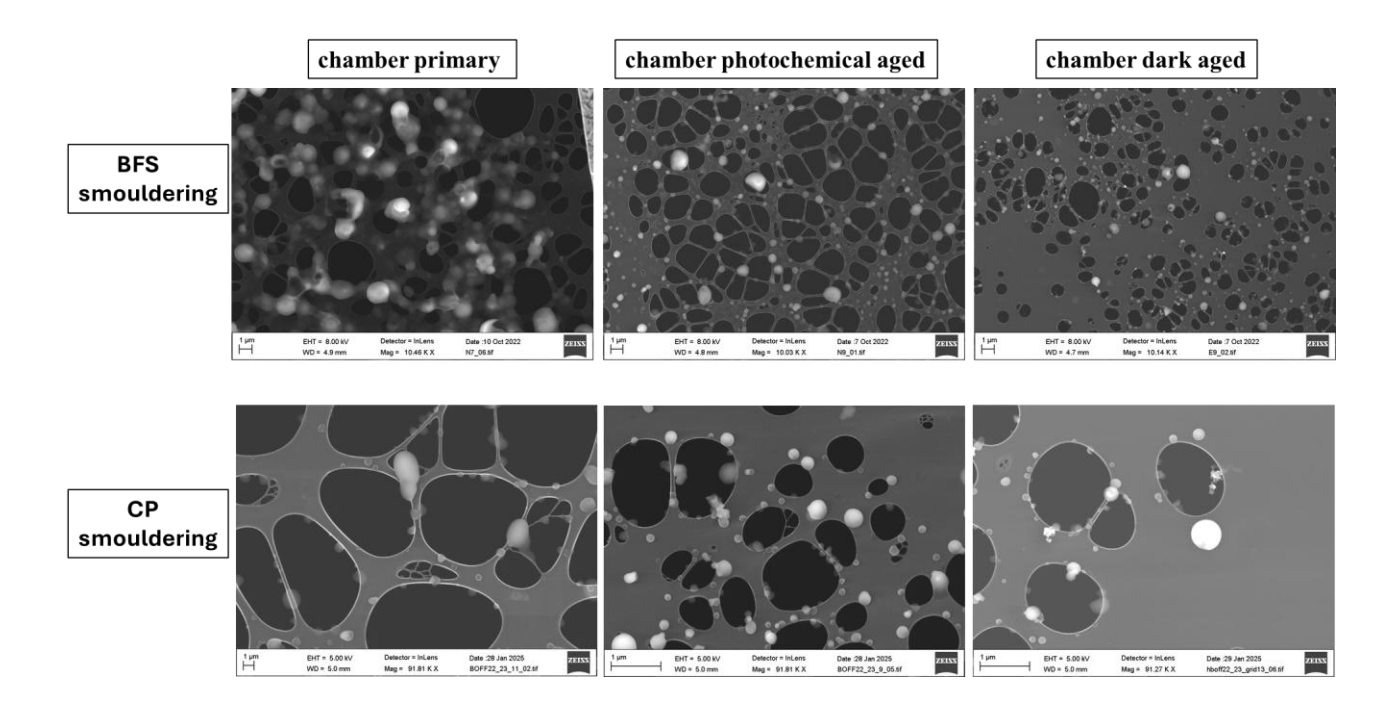


Fig. S15: Representative SEM images of chamber primary and oxidative aged emissions from smouldering combustion of CP and BFS. We observed higher abundance of spherical tarballs in aged samples compared to more amorphous morphology of primary emissions in the chamber.

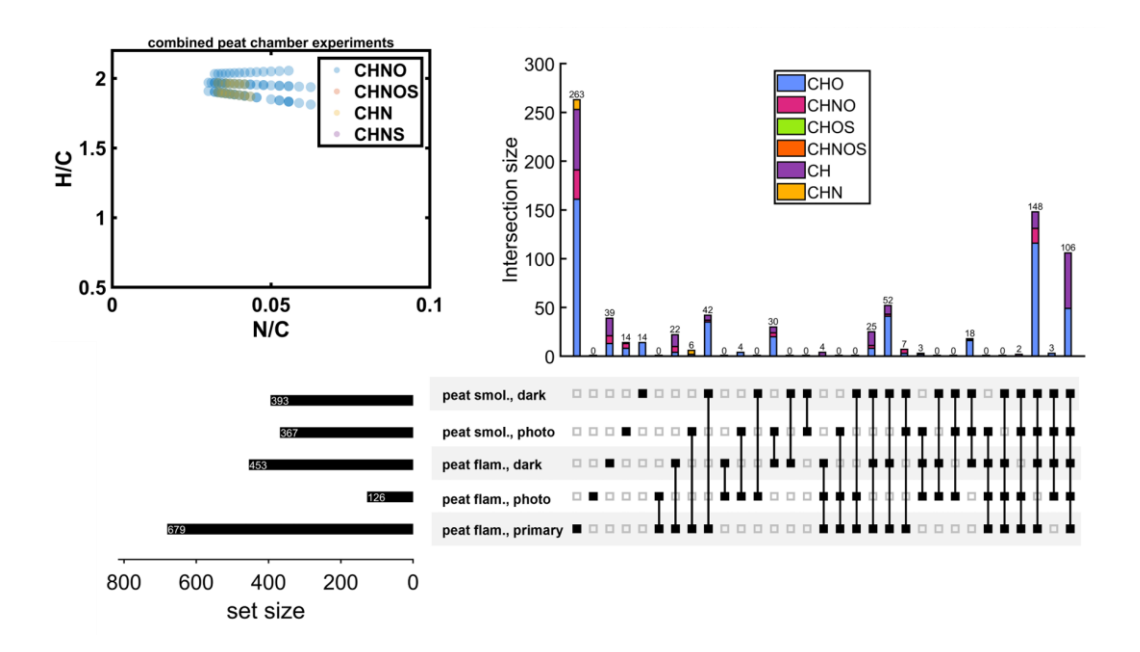


Fig. S16: Upset plot showing the number of unique sum formulae obtained from chamber diluted primary and aged samples from commercial peat (CP) combustions as well as the dominant chemical classes they belong to. Insufficient material on the filters collected from chamber resulted in identification of fewer chemical formulae of only highly abundant chemical groups

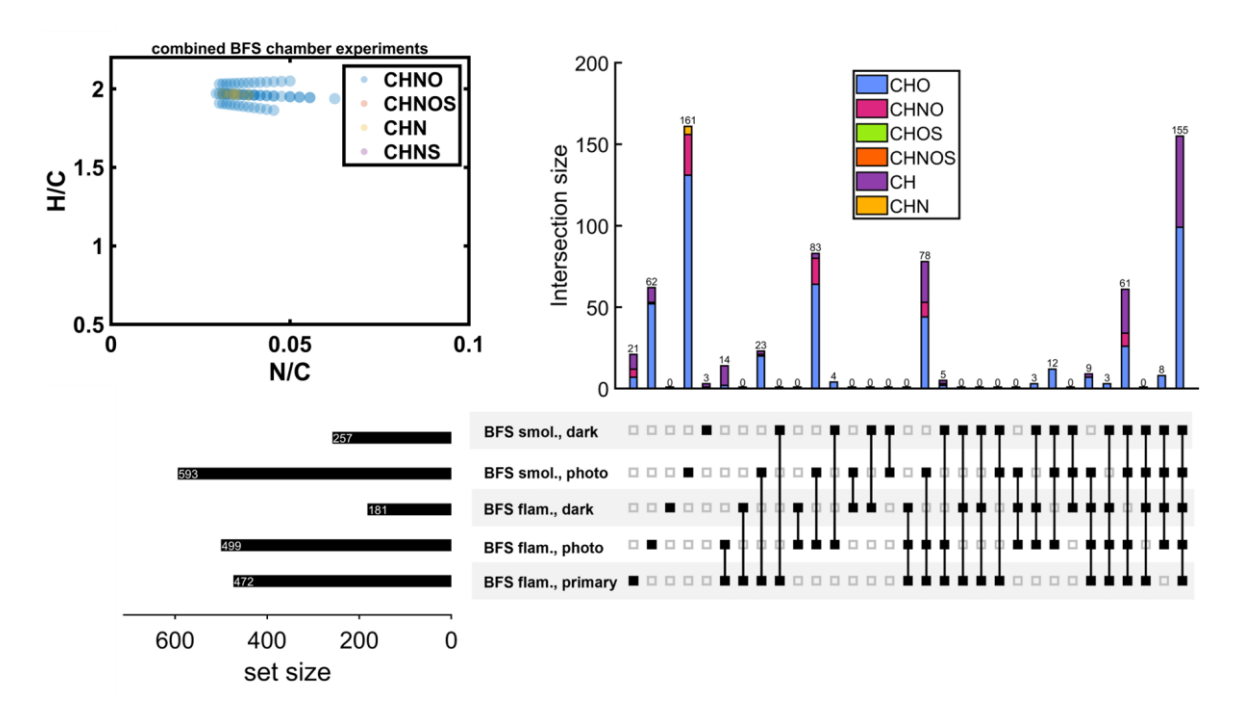


Fig. S17: Upset plot showing the number of unique sum formulae obtained from chamber diluted primary and aged samples from boreal forest surface (BFS) combustions as well as the dominant chemical groups they belong to. Insufficient material on the filters collected from chamber resulted in identification of fewer chemical formulae of only highly abundant chemical groups

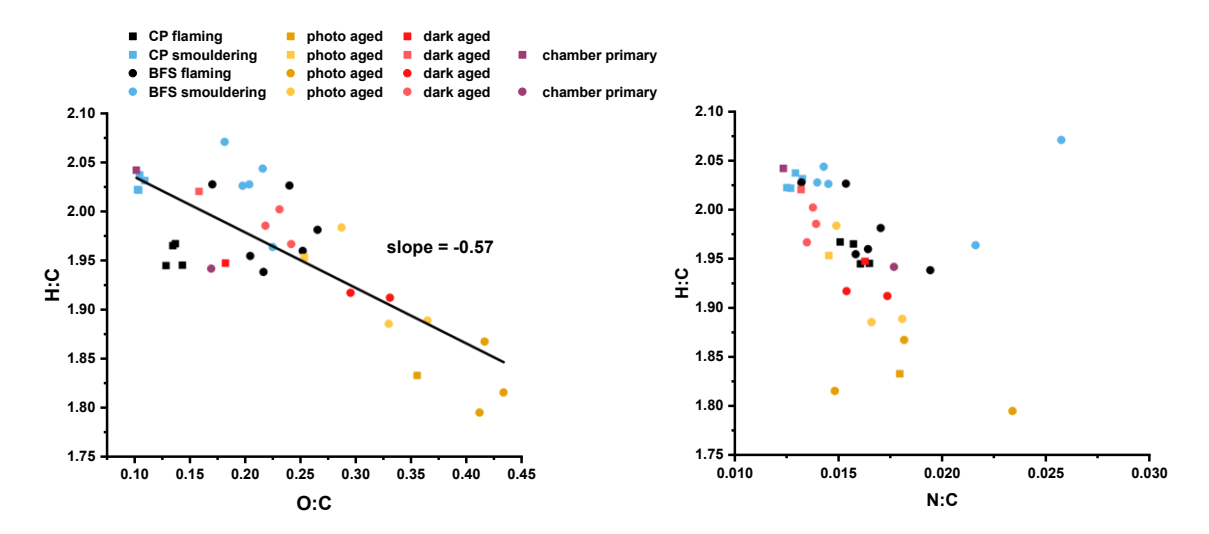


Fig. S18: Van-Krevelen diagrams for H:C vs O:C and H:C vs N:C ratios obtained from HR-AMS from the environmental chamber for CP and BFS combustion experiments. Data obtained for primary emission of flaming (black) and smouldering (grey) burns were compared to the elemental ratios at the end of photochemical (orange for flaming emission, yellow for smoldering emissions) and dark (dark blue for flaming emissions and light blue for smoldering emissions) aging in the chamber.

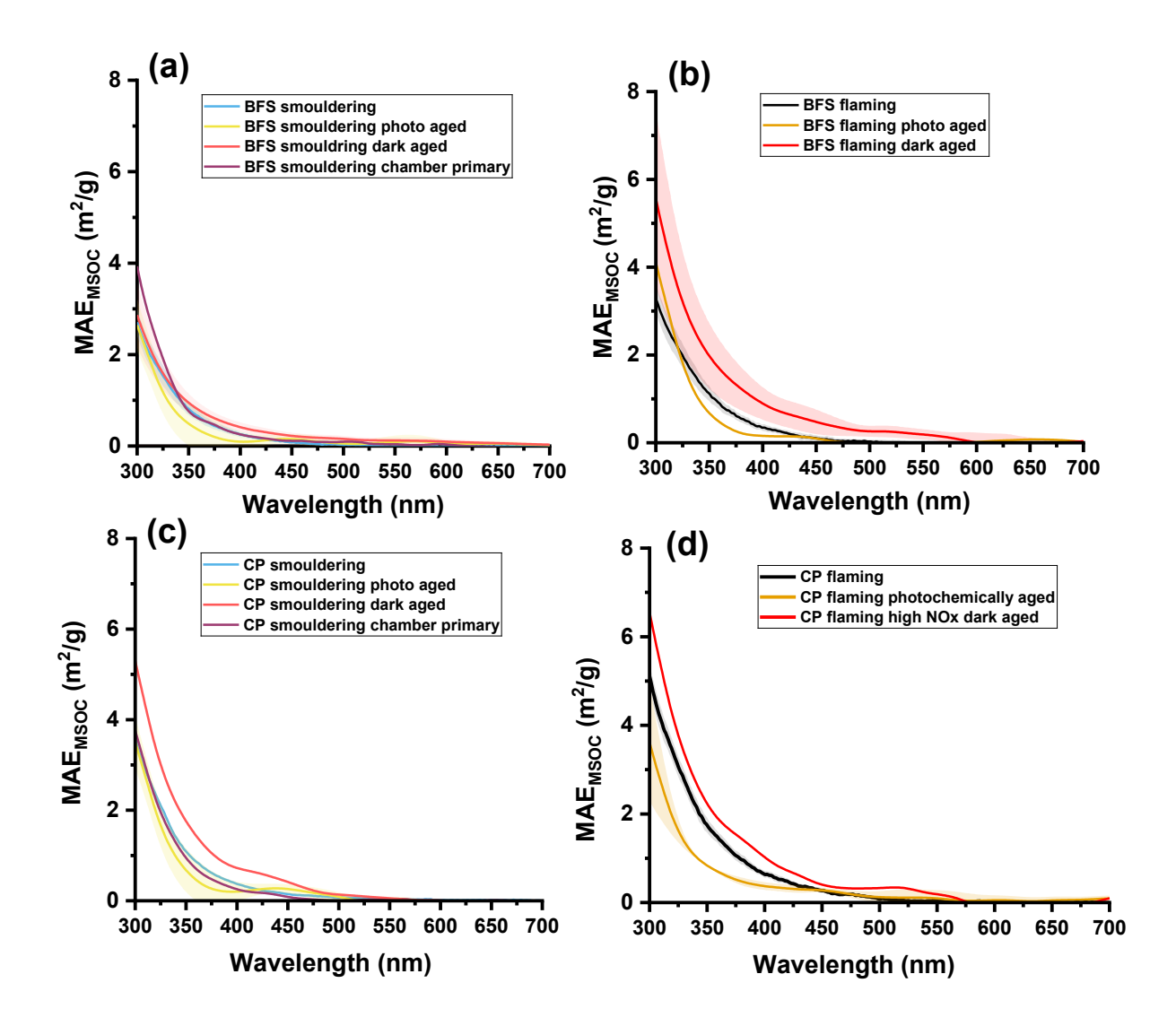


Fig. S19: wavelength dependence of MAE_{MSOC} for (a-b) BFS and (c-d) CP smouldering and flaming emissions. Here we have compared MAE_{MSOC} of fresh emission (black) with photochemically (yellow for smouldering, orange for flaming) and dark aged emission (light red for smouldering and dark red for flaming) in the chamber. Straight line denotes the mean of replicates, while the shaded areas highlight the standard deviation of mean.

Table S1: Origins and compositions of the biomasses used in the experiments

Fuel	Origin (longitude/latitude)	moistur e (%)	composition information (C/N/S/H) %	sampl e mass (g)	
Boreal Forest Surface (BFS)	62.485098"N, 27.491264"E (Kiviniemi)	8.2-16.1	50.5/1.19/0.11/5.4	155- 550	Extra litter 10- 24 g
Commercial Peat (CP)	??	9.7	57/1.92/0.2/5.8	50	
Finnish Peatland (FIA)	61°47'21.6"N, 24°18'35.9"E (Lakkasuo)	-	46.5/-/-	50	
Finnish Peatland (FIB)	61°49'28.0"N, 24°08'25.8"E (Siikaneva)	-	47.6/-/-	50	
Norwegian Peatland (NOR)	78°13'00.0"N, 13°45'00.0"E (Svalbard)	-	27.9/1.85/-/-	50	
Russian Peatland (RUS)	66°33'10.2"N, 60°37'57"E (Rogovaya)	-	51.7/2.9/-/-	50	
Savanna Wood (SW)	26°34'12"S, 26°56'24"E (South Africa)	9.4	48.8/0.88/0.05/5.6	60	
Savanna Grass (SG)	26°34'12"S, 26°56'24"E	8.6	43/0.94/0.10/5.1	50	

Table S2. Components measured by the FTIR and the grouping for the gaseous organic compounds

Component	Formula	Calibration range	Unit	VOC group
Water vapor	H2O	20	%	
Carbon dioxide	CO2	25	%	
Carbon monoxide	CO	5000	ppm	
	CO	10000	ppm	
Nitrous oxide	N2O	200	ppm	
Nitrogen monoxide	NO	1000	ppm	
Nitrogen dioxide	NO2	200	ppm	
Sulfur dioxide	SO2	1000	ppm	
Carbonyl sulfide	COS	100	ppm	
Ammonia	NH3	500	ppm	
Hydrogen chloride	HC1	200	ppm	
Hydrogen cyanide	HCN	100	ppm	
Hydrogen fluoride	HF	100	ppm	
Oxygen	O2	25	%	
Methane	CH4	1000	ppm	Methane
Ethane	C2H6	100	ppm	Aliphatic hydrocarbon
Propane	C3H8	100	ppm	Aliphatic hydrocarbon
Butane	C4H10	100	ppm	Aliphatic hydrocarbon
Pentane	C5H12	100	ppm	Aliphatic hydrocarbon
Hexane	C6H14	100	ppm	Aliphatic hydrocarbon
Heptane	C7H16	100	ppm	Aliphatic hydrocarbon
Octane	C8H18	100		Aliphatic hydrocarbon
Acetylene	C2H2	500	ppm	Aliphatic hydrocarbon
Ethylene	C2H2	500	ppm	Aliphatic hydrocarbon
Propene	C2H4 C3H6	500	ppm	Aliphatic hydrocarbon
1,3-Butadiene	C4H6	500	ppm	Aliphatic hydrocarbon
Benzene	C4H6	500	ppm	Aromatic
Toluene	C7H8	100	ppm	Aromatic
	C8H10	100	ppm	
m-Xylene	C8H10		ppm	Aromatic
o-Xylene	-		ppm	Aromatic
p-Xylene	C8H10 C9H12	100	ppm	Aromatic
1,2,3-Trimethylbenzene	+	100	ppm	Aromatic
1,2,4-Trimethylbenzene	C9H12	100	ppm	Aromatic
1,35-Trimethylbenzene	C9H12	100	ppm	Aromatic
Phenol	C6H6O	200	ppm	Aromatic
Furan	C4H4O	200	ppm	Aromatic
Furfural	C5H4O2	200	ppm	Aromatic
Formic acid	CH2O	100	ppm	Non-aromatic oxygenated
Acetic acid	C2H4O2	200	ppm	Non-aromatic oxygenated
Formaldehyde	СНОН	500	ppm	Non-aromatic oxygenated
Acetaldehyde	C2H4O	100	ppm	Non-aromatic oxygenated
Methanol	CH4O	200	ppm	Non-aromatic oxygenated
Ethanol	С2Н6О	200	ppm	Non-aromatic oxygenated
Propanol	C3H8O	100	ppm	Non-aromatic oxygenated
Methyl tert-butyl ether (MTBE)	C5H12O	100	ppm	Non-aromatic oxygenated

Table S3: Relative abundance of different OC fractions and EC in fresh emission and diluted primary

and aged emissions in teflon chamber

anu	ageu	eiiii	5510	IIS II	ı tei	1011	CHAI	mber 												T						
Fuel	Experiment			fresh emission (% of	total)			chamber diluted primary (% of total)						photo aged in chamber (% of total)							dark aged in chamber (% of total)					
	I	OC1	OC2	£20	OC4	Эd	EC	OC1	OC2	£20	OC4	Эd	EC	120	OC2	£20	OC4	PC	EC	OC1	OC2	£20	OC4	ЪС	EC	
	1a	19.7	24.5	30.4	5.95	13.9	5.54							5.15	9.40	35.5	13.0	34.8	2.15							
	116	20.8	22.2	25.7	5.0	8.67	17.7													7.50	12.5	29.9	12.6	26.2	11.3	
	1c	8.73	11.0	14.1	4.38	5.27	56.5	5.70	10.6	28.1	11.6	4.70	39.3													
CP	1d	22.3	26.5	29.8	6.54	14.3	0.47							6.07	13.9	40.1	12.1	27.8	0.03							
	1e	21.8	27.0	31.6	6:39	12.6	0.65													7.46	14.6	35.8	12.1	30.0	0.01	
	1f	21.6	26.9	29.9	6.21	14.7	99.0	8.6	14.5	36.3	12.1	27.3	0.01													
	2a	23.8	27.7	26.3	4.32	4.39	13.5							6.85	14.0	34.2	12.8	13.0	19.1							
BFS	2b	24.6	26.2	27.7	5.39	4.75	11.4													7.92	13.4	33.5	12.6	13.7	18.8	
	2c	20.3	25.7	26.7	4.62	3.55	19.1	8.03	13.4	33.4	12.3	0.42	32.4													

Fuel	Experiment		fresh emission (% of	total)				chamber diluted primary (% of total)								photo aged in chamber	(% of total)			dark aged in chamber (% of total)					
	1	OC1	OC2	OC3	OC4	PC	EC	OC1	OC2	OC3	OC4	PC	EC	OC1	OC2	OC3	OC4	PC	EC	OC1	OC2	OC3	OC4	PC	EC
	2d	27.5	28.1	28.2	5.10	10.4	0.70							4.73	12.1	41.4	14.6	27.2	0.01						
BFS	2e	23.1	30.6	31.5	5.40	9.00	0.40													8.80	13.2	38.0	14.2	22.2	3.50
	2f	19.1	27.5	29.5	6.34	15.7	1.86	12.1	14.3	37.0	10.8	20.7	5.10												
	3a	24.7	21.6	24.4	7.1	11.5	10.7							13.0	20.8	28.2	9.30	16.0	12.7						
Λ	3b	26.8	23.0	27.3	6.80	7.00	9.10													8.90	16.5	36.4	9.50	25.1	3.60
SW	3c	27.0	26.1	26.3	6.70	8.40	5.60							5.20	13.6	37.0	14.0	30.2	0.01						
	3d	29.2	24.6	22.9	6.20	11.4	5.65													9.2	16.1	34.5	9.1	14.0	17.1
7.5	4a	35.0	24.7	20.6	5.30	8.40	6.0							6.90	14.4	34.0	13.1	31.6	0.01						
98	4b	27.7	26.1	24.1	5.00	8.20	8.90													9.21	16.7	29.8	10.7	12.6	20.9

Fuel	Experiment		fresh emission (% of total)						chamber diluted	primary (% of total)					photo aged in chamber	(% of total)				dark aged in chamber (% of total)					
	ı	OC1	OC2	OC3	OC4	PC	EC	OC1	OC2	620	OC4	ЪС	EC	120	OC2	OC3	OC4	PC	EC	120	OC2	OC3	OC4	Эd	EC
75	4c	31.6	27.1	25.0	4.20	8.50	3.60							5.42	8.97	18.7	8.22	17.5	41.2						
SS	4d	27.3	26.2	26.5	4.80	09.6	5.60													10.9	15.8	30.4	10.3	27.2	5.40

Table S4: MAE,k in fresh and chamber aged BB emissions along with effective density of bulk BB aerosol (mean \pm standard deviation)

Experiment No.	Fuel	Combustion Condition (no. of replicates)	MAE _{MISOC_368} (m² g ⁻¹) (fresh emission)	k _{MSOC_550} (fresh emission)	$\mathrm{MAE_{WSOC_365}}$ (m ² g ⁻¹) (fresh emission)	kwsoc_sso (fresh emission)	density (g cm³) (chamber primary)	Aging condition (in chamber)	MAE _{MSOC_365} (m ² g ⁻¹) (chamber aged)	k _{MSOC_550} (chamber aged)	MAEwsoc_365 (m² g¹) (chamber aged)	kwsoc_sso (chamber aged)	density (g/cm³) (chamber aged)
la		flaming $(n=2)$	1.32 ± 0.16	0.007±0.001	1.59 ± 0.14	0.012 ± 0.001	NA	photo aged	0.65 ± 0.07	0.003±0.002	1.49 ± 0.27	0.0078± 0.001	1.30 ± 0.05
116		Flaming $(n = 1)$	1.31	0.007	0.78	0.007	1.10	high NOx	1.75	0.01	0.62	0.003	1.10
1c	Commercial Peat (CP)	flaming $(n = 1)$	NaN	NaN	NaN	NaN	NA	no aging	NaN	sNaN	NaN	NaN	NaN
14	Commerci	smouldering $(n = 2)$	0.76 ± 0.02	0.004 ± 0.00	1.45 ± 0.32	0.010 ± 0.002	1.00 ± 0.02	photo aged	1.56 ± 0.69	0.009 ± 0.005	0.48 ± 0.011	0.002 ± 0.000	1.20 ± 0.03
1e		smouldering $(n = 1)$	NaN	NaN	NaN	NaN	1.10	high NOx	1.29	0.007	0.77	0.005	1.10
1f		smouldering $(n = 1)$	0.78	0.004	1.43	0.011	NaN	no aging	0.61	0.003	0.34	0.002	NA
2a	face (BFS)	flaming (n = 3)	0.71 ± 0.15	0.004 ± 0.001	0.69 ± 0.13	0.004 ± 0.001	1.20 ± 0.05	photo aged	0.71 ± 0.22	0.003 ± 0.001	0.75 ± 0.12	0.002± 0.001	1.30 ± 0.09
2b	Boreal forest surface (BFS)	flaming $(n = 3)$	0.75 ± 0.04	0.004 ± 0.000	0.88 ± 0.36	0.006 ± 0.003	1.20 ± 0.05	high NOx dark	2.21 ± 1.23	0.014 ± 0.009	0.82 ± 0.08	0.004 ± 0.003	1.30 ± 0.07

2c		flaming $(n=1)$	0.95	0.005	9.65	0.004	NaN	no aging	NaN	NaN	NaN	NaN	NaN
2d	urface (BFS)	smouldering $(n = 3)$	0.62 ± 0.11	0.003 ± 0.001	1.17 ± 0.26	0.006 ± 0.002	1.20 ± 0.1	photo aged	0.50 ± 0.06	0.002 ± 0.000	0.26 ± 0.04	0.001 ± 0.000	1.30 ± 0.05
2e	Boreal forest surface (BFS)	smouldering $(n = 3)$	0.48 ± 0.05	0.002 ± 0.005	0.78 ± 0.11	0.005 ± 0.001	1.10 ± 0.03	high NOx	0.65 ± 0.11	0.003 ± 0.001	0.60 ± 0.04	0.002 ± 0.001	1.10 ± 0.03
2f		smouldering $(n = 1)$	0.58	0.003	0.92	900.0	1.20	no aging	0.64	0.022	0.31	0.002	1.20
3a		$flaming \\ (n = 1)$	1.38	0.011	1.28	600.0	1.40	photo aged	1.06	0.007	1.03	0.003	1.40
36	Savanna wood (SW)	flaming $(n=1)$	1.06	0.009	1.08	0.008	1.50	low NOx	NaN	NaN	1.22	0.007	1.30
3с	Savanna v	smouldering $(n = 1)$	1.11	600.0	1.03	0.007	NA	photo aged	89:0	0.004	0.40	0.001	1.40
3d		smouldering $(n = 1)$	1.05	0.008	0.85	0.007	1.40	low NOx	0.73	0.006	98.0	0.005	1.40
4a		flaming $(n = 1)$	0.89	600.0	1.22	0.01	1.80	photo aged	1.35	0.005	3.43	0.012	1.60
4b	Savanna grass (SG)	flaming $(n=1)$	0.93	600.0	0.94	0.008	1.70	low NOx	1.21	0.01	1.56	0.008	1.50
4c	Savanna g	smouldering $(n = 1)$	0.94	0.012	0.84	900.0	1.70	photo aged	NaN	NaN	2.10	0.010	1.40
4d		smouldering $(n = 1)$	89.0	0.005	1.18	0.011	1.60	low NOx	1.32	0.01	0.83	0.005	1.50

References:

- Descals, A., Gaveau, D. L. A., Verger, A., Sheil, D., Naito, D., & Peñuelas, J. (2022). Unprecedented fire activity above the Arctic Circle linked to rising temperatures. *Science*, *378*(6619), 532–537. https://doi.org/10.1126/science.abn9768
- Huang, X., & Rein, G. (2017). Downward spread of smouldering peat fire: the role of moisture, density and oxygen supply. *International Journal of Wildland Fire*, 26(11), 907. https://doi.org/10.1071/WF16198
- Jain, P., Barber, Q. E., Taylor, S. W., Whitman, E., Castellanos Acuna, D., Boulanger, Y., Chavardès, R. D., Chen, J., Englefield, P., Flannigan, M., Girardin, M. P., Hanes, C. C., Little, J., Morrison, K., Skakun, R. S., Thompson, D. K., Wang, X., & Parisien, M.-A. (2024). Drivers and Impacts of the Record-Breaking 2023 Wildfire Season in Canada. *Nature Communications*, 15(1), 6764. https://doi.org/10.1038/s41467-024-51154-7
- Mukherjee, A., Hartikainen, A., Joutsensaari, J., Basnet, S., Mesceriakovas, A., Ihalainen, M., Yli-Pirilä, P., Leskinen, J., Somero, M., Louhisalmi, J., Fang, Z., Kalberer, M., Rudich, Y., Tissari, J., Czech, H., Zimmermann, R., & Sippula, O. (2024). Black carbon and particle lung-deposited surface area in residential wood combustion emissions: Effects of an electrostatic precipitator and photochemical aging. Science of The Total Environment, 952, 175840. https://doi.org/10.1016/j.scitotenv.2024.175840
- Schneider, E., Rüger, C. P., Chacón-Patiño, M. L., Somero, M., Ruppel, M. M., Ihalainen, M., Köster, K., Sippula, O., Czech, H., & Zimmermann, R. (2024). The complex composition of organic aerosols emitted during burning varies between Arctic and boreal peat. *Communications Earth and Environment*, 5(1). https://doi.org/10.1038/s43247-024-01304-y
- Vakkari, V., Beukes, J. P., Dal Maso, M., Aurela, M., Josipovic, M., & van Zyl, P. G. (2018). Major secondary aerosol formation in southern African open biomass burning plumes. *Nature Geoscience*, 11(8), 580–583. https://doi.org/10.1038/s41561-018-0170-0
- Vakkari, V., Vettikkat, L., Kommula, S., Mukherjee, A., Hao, L., Backman, J., Buchholz, A., Gawlitta, N., Ihalainen, M., Jaars, K., Köster, K., Le, V., Miettinen, P., Nissinen, A., Czech, H., Alton, M., Passig, J., Peltokorpi, S., Piedehierro, A. A., Pullinen, I., Rosewig, E. I., Schobesberger, S., Shukla, D., Siebert, S. J., Somero, M., Virkkula, A., Welti, A., Yli-Pirilä, P., Ylisirniö, A., Zimmermann, R., van Zyl, P. G., Virtanen, A., & Sippula, O. (2025). Laboratory experiments on savannah and European boreal forest fire emissions. *Journal of Geophysical Research: Atmospheres, under revision*
- van Wees, D., van der Werf, G. R., Randerson, J. T., Rogers, B. M., Chen, Y., Veraverbeke, S., Giglio, L., & Morton, D. C. (2022). Global biomass burning fuel consumption and emissions at 500 m spatial resolution based on the Global Fire Emissions Database (GFED). *Geoscientific Model Development*, 15(22), 8411–8437. https://doi.org/10.5194/gmd-15-8411-2022
- Walker, X. J., Rogers, B. M., Veraverbeke, S., Johnstone, J. F., Baltzer, J. L., Barrett, K., Bourgeau-Chavez, L., Day, N. J., de Groot, W. J., Dieleman, C. M., Goetz, S., Hoy, E., Jenkins, L. K., Kane, E. S., Parisien, M.-A., Potter, S., Schuur, E. A. G., Turetsky, M., Whitman, E., & Mack, M. C. (2020). Fuel availability not fire weather controls boreal wildfire severity and carbon emissions. *Nature Climate Change*, 10(12), 1130–1136. https://doi.org/10.1038/s41558-020-00920-8